Biomaterials 126 (2017) 49–60

Contents lists available at ScienceDirect

Biomaterials

journal homepage: www.elsevier.com/locate/biomaterials

TLR4/MD2 specific peptides stalled *in vivo* LPS-induced immune exacerbation

Seolhee Park [1], Hyeon-Jun Shin [1], Masaud Shah [1], Hey-Young Cho, Muhammad Ayaz Anwar, Asma Achek, Hyuk-Kwon Kwon, Byugsung Lee, Tae Hyeon Yoo, Sangdun Choi*

Department of Molecular Science and Technology, Ajou University, Suwon, 443-749, South Korea

ARTICLE INFO

Article history:
Received 3 January 2017
Received in revised form
15 February 2017
Accepted 17 February 2017
Available online 20 February 2017

Keywords:
Biopanning
In silico
Peptide drug
Phage display
Proinflammatory cytokine
Toll-like receptor

ABSTRACT

Negative regulation of Toll-like receptor-4 (TLR4) is anticipated to control the pathogen-induced exaggerated immune response. However, effective TLR4 antagonists with scarce off-target effects are yet to be developed. To fill this void, we sought to design small peptide-inhibitors of the TLR4/MD2–LPS interaction. Here we report novel TLR4-antagonistic peptides (TAP), identified through phage display, endowed with the LPS-induced proinflammation inhibition, and confirmed in mice. TAPs-attributed TLR4-antagonism were initially evaluated through NF-κB inhibition in HEK-blue hTLR4 and RAW264.7 cells, and further reinforced by the downregulation of MAPKs (mitogen-activated protein kinases), NF-κB, interleukin 6, and suppression of the oxidative-stress products and iNOS in macrophages and human peripheral blood mononuclear cells (hPBMCs). Among these, TAP2 specifically halted the TLR4, but not other TLRs signaling, which was further confirmed by the biophysical kinetic assay. Finally, TAP2 diminished LPS-elicited systemic cytokine response *in vivo*, suggesting that TAPs, specifically TAP2, have the potential to treat TLR4-mediated immune ailments.

1. Introduction

TLR4 is endowed with the capacity to activate the innate immune signaling cascade via both myeloid differentiation primary response protein 88 (MyD88)-dependent and MyD88-independent pathways. TLR4 is mainly activated by lipopolysaccharide (LPS) recognition through accessory molecules such as LPS-binding protein (LBP), the cluster of differentiation 14 (CD14), and myeloid differentiation factor 2 (MD2) [1]. Stimulation of TLR4 through the MyD88-dependent signaling pathway leads to the early phase activation of nuclear factor κB (NF-κB) and mitogen-activated protein kinases (MAPKs); these events result in the secretion of proinflammatory cytokines such as interleukin 1β (IL-1β), IL-6, and tumor necrosis factor α (TNF-α) [2,3]. Unlike MyD88-dependent pathway, the TRAM/TRIF-dependent route of TLR4 signaling leads to late-phase activation of interferon-regulatory factors (IRFs) and NF-κB, resulting in the secretion of type I interferons (IFN) [4,5]. Besides, LPS-induced TLR4 activation is also reported to cause oxidative stress in macrophages via nitric oxide (NO) and reactive oxygen species (ROS) [6,7]. These signaling pathways, if regulated in their threshold, provide a crucial defensive role and contribute to the host survival by engaging the dangers. However, if dysregulated or over activated and left unchecked, this system put host in extreme danger by activating multiple immune-related disorders [8]. Therefore, countering uncontrolled TLR-mediated signaling has been a major subject of research in the last decade or more [9].

Disturbance in the activation of TLR4 may lead to the initiation or further aggravation of various human illnesses, such as autoimmune diseases, inflammatory diseases, and cancers [10–13]. To address this problem, TLR4-targeting compounds have been actively developed, and some are in clinical trials as agents that can reduce the severity of TLR4-related diseases [14,15]. Many TLR4 agonists and antagonists have been obtained by modifying the main scaffold structure of lipid A [16,17]. For instance, the number of acyl chains or phosphate groups of lipid A switches between TLR4/MD2 agonistic (six chains) [18] and antagonistic activity (lipid IVa) [19]. Eritoran, lipid A, and *Rhodobacter sphaeroides* lipid A (RsLA) can block the interaction of LPS with MD2 and prevent LPS-

* Corresponding author.
E-mail address: sangdunchoi@ajou.ac.kr (S. Choi).
[1] These authors contributed equally to this work.

http://dx.doi.org/10.1016/j.biomaterials.2017.02.023
0142-9612/

induced shocks in mice [20,21]. Recently a new type of molecule that bears no structural similarity to lipid A or lipid A-derived compounds has been reported. This peptidomimetic compound, Neoseptin-3, activates mouse TLR4 in MyD88- and TRIF-dependent manner [22]. Most TLR4 (ant)agonists have been reported to interact with the ectodomain or MD2 and modulate downstream signaling. However, significant progress has been made in the search for inhibitors of TLR4, and cytoplasmic domain (TIR domain)-targeting molecules and small peptides that block the downstream TLR4 pathway have also been identified (as reviewed in our previous studies [14,15]). As one example, TAK-242 is a molecule that inhibits the protein-protein interaction between TLR4 and TIRAP/TIRAM and blocks downstream signaling [23,24].

Small peptides are structurally versatile elements that have been identified through various techniques, such as yeast two-hybrid assay and phage display (Ph.D.); small peptides are often designed to mimic or oppose the activity of PAMPs and to complimentarily interact with the target proteins [25–27]. These peptides have attracted interest in the field of peptide therapeutics and vaccine adjuvants. The Ph.D. technology is generally used to identify novel peptides in phage libraries that can bind to the proteins of choice [28]. Ph.D. has been widely utilized in finding reagents, diagnostics, and therapeutics since the establishment of this technique by George P. Smith [29–31]. A modified phage is constructed in this method by fusing the corresponding gene fragments with phage coat-expressing gene, thereby allowing the peptides to be displayed on the phage surface. Engineering of the M13 coat protein has substantially moved the Ph.D. platform forward [30]. Alizadeh et al. have recently reported small peptides through Ph.D. that bind to TNF-α and neutralize its cytotoxicity [32]. Similarly, a 13-mer peptide has been selected through Ph.D. that binds to Clec9a on mouse DCs and activates $CD8^+$ cells and IFNγ secretion. This peptide has been reported to reduce lung metastasis and could work as an antigen delivery caries in cancer immunotherapy [33]. Ph.D. technique has also been invested to develop peptide-based nanosensors that can detect pentaerythritol- tetranitrate (PETN) and its surrogate PETNH [34]. Peptides are thought to have fewer side effects than regular drugs do and are easy to modify, which can elicit or suppress TLR4 signaling in a more specific manner [25,35]. Multiple studies have been conducted with an aim to standardize screens for TLR4-antagonistic peptides that bind to the ecto- or cytoplasmic domain of TLR4. One study utilized a computational method and derived some peptides from MD2. These peptides are believed to block TLR4-MD2 interaction and inhibit LPS-induced TLR4 signaling [26]. Another group used a decoy approach and selected small TRAM-derived peptides that effectively block TLR4 signaling [36].

Nonetheless, the issues with the pharmacodynamics and pharmacokinetics of peptide drugs stress the importance of their stability. Compared to that of small molecule and monoclonal antibody therapeutics, one of the drawbacks of peptide drugs is their vulnerability to proteolytic degradation [37]. However, this could be overcome by altering the amide bonds and side chains of the amino acids, to generate proteolytic-resistant peptidomimetics [38]. Cyclization and structural constrains can also improve the stability of the peptides [39]. Crossing biological barriers is another issue for peptide drugs that can be resolved by the addition of carrier molecules [40]. For example, cell and tissue penetration can be facilitated by adding positively charged amino acids to the peptide terminus [41]. In addition, covalent modifications, like macro- and nanoparticle-mediated peptide assemblies have also improved targeting efficiencies [40]. In some cases, the oral availability of the peptides can be disregarded. For example, the peptide hormones amylin, insulin, somatostatin, and human growth hormone can be administered subcutaneously. The development of peptide drugs and their therapeutic potentials are increasing rapidly. This overburdens chemical biologists to improve the suboptimal parameters of these peptides and educate biotechnology investors and commercial drug developers about the misconceptions related to peptide drugs.

Considering that small peptides are more convenient to bind to their target, we employed the same technique and identified three novel peptides that halt the LPS induced TLR4 pathway. The selected TLR4-antagonizing peptides (TAPs) suppress the LPS-induced secretion of IL-6, inhibit the production of oxidative-stress markers (NO and ROS) and block the downstream signaling pathway of TLR4 in RAW264.7 and human peripheral blood mononuclear cells. Biophysical and molecular docking analysis suggested that these peptides preferentially bind to TLR4/MD2 and likely hinder the LPS access to MD2. The TLR4 antagonistic effect of TAP also confirmed in mouse model, which inhibited the LPS elicited systemic cytokines response.

2. Materials and methods

2.1. Construction and enrichment of the TLR4/MD2 binding peptide library

A 15-mer peptide library was synthesized with forward primer 5′-TTG ATC GCA AGG ATC GGC TAG C-3′ and reverse primer 5′-AA GGC CTT GGT ACC GCT GCC ACC $(MNN)_{15}$ GCT AGC CGA TCC TTG CGA TCA A-3′. These two primers were annealed by incubation for 10 min at 95 °C, 30 s at 90 °C, 30 s at 85 °C, 30 s at 80 °C, 30 s at 75 °C, 30 s at 70 °C, 30 s at 65 °C, 30 s at 60 °C, 30 s at 55 °C, 30 s at 50 °C, 30 s at 45 °C, 30 s at 40 °C, and 30 s at 35 °C, and then elongated using *Pfu* DNA polymerase (SolGent, Daejeon, Korea) for 30 min at 68 °C. The DNA product was digested with *Nhe*I/*Kpn*I and cloned into the fUSE55 vector with T4 DNA ligase (New England Biolabs, Inc., Ipswich, MA, USA). The DNA library was transformed into electrocompetent *Escherichia coli* (*E. coli*) DH10B cells, generating 6.6×10^7 distinct clones. The phage library DNA was transformed into electrocompetent *E. coli* TG-1 cells and recovered in 10 ml of SOC. The recovered TG-1 cells were transferred to 1 l of 2 × YT medium containing 20 μg/ml tetracycline and incubated at 37 °C overnight. After centrifugation (9300 × *g*, 15 min, 4 °C), the supernatant was transferred to a clean bottle. Then, 1/5 volume of 20% PEG/2.5 M NaCl was added to the supernatant and incubated at 4 °C overnight. The phage pellet was collected after centrifugation (9300 × *g*, 15 min, 4 °C) and resuspended in 15 ml of TBS, and then centrifuged again (12000 × *g*, 10 min, 4 °C) to remove residual cells. Then, 1/5 volume of 20% PEG/2.5 M NaCl was added to the supernatant and incubated on ice for 1 h. Finally, the phage pellet was collected after centrifugation (12000 × *g*, 10 min, 4 °C) and resuspended in 3 ml of TBS. The 12-mer peptide library was synthesized with forward primer 5′-GCC CAG CCG GCC ATG GCC $(NNK)_{12}$ TCG AGT GGT GGA GGC GGT TCA G-3′ and reverse primer 5′-GCC AGC ATT GAC AGG AGG TTG AG-3′. The two primers were annealed and elongated as described above. Then, the DNA product was digested with *Nco*I/*BamH*I and cloned into the pHEN2 phagemid vector with T4 DNA ligase. The library was then transformed into electrocompetent *E. coli* DH10B cells, generating 2.0×10^9 distinct clones. The phage library was transformed into *E. coli* XL1-Blue cells and recovered in 10 ml of SOC. Recovered XL1-Blue cells were transferred to 1 l of 2 × YT medium containing 100 μg/ml ampicillin and incubated overnight at 37 °C. The culture was transferred to 500 ml of fresh 2 × YT medium and grown at 37 °C until the OD_{600} reached 0.5. The hyperphage, M13K07ΔpIII (PROGEN Biotechnik GmbH, Heidelberg, Germany), was then added to 25 ml of culture (final concentration, 1×10^{12} Pfu/ml). After incubation at 37 °C for 30 min, the cell pellet was collected by centrifugation (3300 × *g*,

10 min, 4 °C) and resuspended in 30 ml of fresh 2 × YT (100 μg/ml ampicillin and 25 μg/ml kanamycin). The cells were grown at 30 °C overnight. Phage particles were recovered as described above.

2.2. Panning procedure

Biopanning was performed as described previously in the Griffin-1 library (Griffin H., MRC, Cambridge, UK, unpublished data) with some modifications [42]. The recombinant human TLR4/MD2 complex (5 μg/ml) that was resuspended in coating buffer (0.05 M Na_2CO_3 pH 9.6) was coated into Nunc MaxiSorp 96-well plates (Thermo Fisher Scientific Inc., Waltham, MA, USA) and refrigerated overnight. After blocking with 5% skim milk in PBS at room temperature (RT) for 2 h, we exposed the wells to the phage libraries (final concentration of 5% skim milk in PBS with 0.05% Tween 20 [PBST]) for 2 h at RT. The bound phages were eluted with 100 μl of elution buffer (100 mM HCl) and neutralized with $^1/_8$ volume of 1 M Tris HCl pH 11 after a wash with PBST. Phage titer was calculated by colony-forming units (cfu) in *E. coli* TG1 for 15-mer libraries and in *E. coli* XL-1 Blue for 12-mer libraries on Luria-Bertani (LB) agar plates containing tetracycline (200 μg/ml) and ampicillin (10 μg/ml), respectively. After that, the phages were amplified in *E. coli* TG1 and XL-1 Blue for the respective libraries and were purified by polyethylene-glycol (PEG)/NaCl precipitation [43] for the subsequent rounds of panning. In each round (total five rounds), the input and output ratio was calculated to estimate the enrichment efficiency.

2.3. High-throughput screening (HTS)

The isolated stand-alone colonies of the transfected cells were collected from LB/Tet (for 15-mer) and LB/Amp (for 12-mer) agar plates into U-bottom 96-well plates, and grown overnight at 37 °C after the fifth round of biopanning. This was followed by stock preparation on LB/Tet or LB/Amp agar plates and centrifugation (at 3000 × *g* for 30 min) for phage preparation in the supernatant. The supernatant that was mixed with an equal volume of binding buffer (10% skim milk in PBST) was added to TLR4/MD2-positive (1.25 μg/ml) and TLR4/MD2-negative 96-well plates (blocked) to check the phage-binding affinity. The wells were blocked with blocking buffer (5% skim milk in PBS) for 2 h and then washed with PBST. After 1 h of the binding reaction at RT, unbound phages were removed by extensive washing with PBST. The bound phages were detected by incubation with 100 μl of an anti-M13 antibody conjugated with horseradish peroxidase (HRP) and subsequent washing with PBST to remove the unbound antibody. Tetramethylbenzidine (100 μl; Thermo Fisher Scientific Inc.) was added to each well and the mixture was kept at RT until a noticeable colour appeared. Next, 1 N H_3PO_4 (100 μl) was added to each well to stop the reaction. Phages showing high binding affinity were selected using ELISA (BioTek Instruments, Inc., Winooski, VT, USA), with analysis of absorbance at 450 nm, and were used for further experiments.

2.4. DNA sequencing and peptide synthesis

The phages that were selected in the ELISA assay were prepared in sufficient quantity to isolate phage DNA, using the Miniprep Kit (GeneAll Biotechnology, Seoul, Korea), and sequenced by Macrogen, Inc. (Seoul, Korea), using the following primers: 5′-TGA ATT TTC TGT ATG AGG-3′ (15-mer, TAP1) and 5′-TTG TGA GCG GAT AAC AAT TTC-3′ (12-mer). The DNA sequences were translated into amino acid sequences and aligned to assess the variation using BioEdit software [44]. The peptides showing high binding affinity for TLR4/MD2 were synthesized by PEPTRON (Daejeon, Korea) with purity greater than 95%. The peptide stocks were dissolved in water (15-mers) and dimethyl sulfoxide (12-mer, TAP2 and 3) at the final concentration of 10 mg/ml and were stored in appropriate aliquots at −20 °C until analysis.

2.5. Cell culture optimization

HEK-Blue™ hTLR4 cells (InvivoGen, San Diego, CA, USA) were cultured in Dulbecco's modified Eagle's medium (DMEM; Thermo Fisher Scientific Inc.) and incubated (humidified atmosphere of 5% CO_2 at 37 °C; Thermo Fisher Scientific Inc.). The medium was supplemented with 10% fetal bovine serum (FBS; Thermo Fisher Scientific Inc.), penicillin (50 IU/ml), streptomycin (50 μg/ml, Thermo Fisher Scientific Inc.), Normocin (100 mg/ml, InvivoGen), and a HEK-Blue selection mixture of antibiotics (2 ml per 500 ml; InvivoGen). Mouse macrophage RAW264.7 cells (ATCC, Manassas, VA, USA) were cultured in Low-Glucose DMEM (Thermo Fisher Scientific Inc.) supplemented with 10% FBS, penicillin (100 IU/ml), and streptomycin (100 μg/ml) in an incubator system. Human peripheral blood mononuclear cells were purchased from PromoCell (Heidelberg, Germany) and cultured in RPMI1640 medium containing 10% FBS, 1% penicillin/streptomycin (Thermo Fisher Scientific Inc.) and 1% L-glutamine (Gibco, Grand Island, NY, USA). LPS was purchased from Sigma-Aldrich Co. (St. Louis, MO, USA), and PAM_3CSK_4, FSL-1, Poly(I:C), R848 and CpG-ODN were purchased from InvivoGen.

2.6. TLR4 induced SEAP detection in peptides treated cells

HEK-Blue™ hTLR4 cells were seeded in 96-well plates at 10^4/well and grown in an incubator for two days. The supernatant was removed, and the cells were treated with TAPs in HEK-Blue detection media (IvivoGen) followed by LPS (20 μg/ml) treatment 1 h later. After 24 h, the culture supernatants were collected and placed in a new 96-well plate. SEAP production was determined as the absorbance of supernatant was measured at 630 nm with the VersaMax Microplate Reader (Molecular Devices Inc., Sunnyvale, CA, USA).

2.7. Cell toxicity quantification of the selected TAPs

Cell viability was measured using MTT solution (Sigma-Aldrich Co.) diluted in PBS. The diluted MTT solution (final concentration: 500 μg/ml) was added (100 μl/well) to the wells, followed by 3 h of incubation at 37 °C. Later, the MTT solution was removed, and a dimethyl sulfoxide solution (100 μl/well; Sigma-Aldrich Co.) was added. After 30 min, the absorbance was measured on a microplate spectrophotometer system (Molecular Devices Inc.) at 540 nm.

2.8. Protein quantification and detection in TAP treated cells

A mixture of the whole-protein extraction solution (M-PER; Thermo Fisher Scientific Inc.) with protease and phosphatase inhibitor cocktail (Thermo Fisher Scientific Inc.) was added to cell pellets. The pellets were kept on ice for 10 min before centrifuging the lysates at 16,000 × *g* for 10 min. Cytoplasmic and nuclear protein extracts were obtained using NE-PER Nuclear and Cytoplasmic Extraction Reagents (Thermo Fisher Scientific Inc.) following the manufacturer's protocol. The protein concentration was measured using the BCA kit (Sigma-Aldrich Co. LLC). Equal amounts of protein were separated on SDS-polyacrylamide gel and were transferred to a Hybond-ECL nitrocellulose membrane (Amersham Pharmacia Biotech, Inc., Piscataway, NJ, USA). The membranes were blocked with 0.05% nonfat dried milk in deionized water for 1 h. The membranes were immunoblotted with

primary specific antibodies against iNOS (BD Biosciences, San Jose, CA, USA), HDAC1 (Merck Millipore, Billerica, MA, USA), NF-κB (p65), IκBα, p-ERK, ERK, p-JNK, JNK, p-p38, p38, ATF3, β-actin (Santa Cruz Biotechnology, Inc., Dallas, TX, USA), p-p65 (Cell Signaling Technology, Danvers, Massachusetts, USA) with gentle shaking overnight at 4 °C. After rigorous washing with PBST, membranes were incubated with anti-mouse/-rabbit HRP-conjugated secondary antibodies (Thermo Fisher Scientific Inc.) for 2 h. The proteins were detected using the SuperSignal West Pico ECL solution (Thermo Fisher Scientific Inc.) and visualized using a Fuji LAS-3000 system (Fujifilm, Tokyo, Japan).

2.9. IL-6, TNF-α and NO secretion

These parameters were measured using the Mouse IL-6 or TNF-α ELISA kit Ready-SET-Go! (eBioscience, San Diego, CA, USA) and Nitric Oxide Detection Kit (iNtRON Biotechnology, Gyeonggi, Korea) from culture supernatants. The absorbance was measured at 450 nm for IL-6 or TNF-α and 540 nm for NO on a microplate reader spectrophotometer (Molecular Devices Inc.), and the data were analyzed against a standard curve using SoftMax Pro 5.3 software (Molecular Devices Inc.).

2.10. ROS quantification in the cytosol and mitochondria

The cells were treated with DAF-FM (Invitrogen Corp., CA, USA) and incubated for 1 h. Next, the cells were harvested by centrifugation at 200 × *g* for 5 min and transferred to brown tubes and kept in PBS at 4 °C. Cytosolic ROS were quantified using DCF-DA (Invitrogen Corp.) staining for 30 min, and mitochondrial ROS were quantified using MitoSOX staining (Invitrogen Corp.) for 10 min. Incubation was followed by cell harvesting and centrifugation at 200 × *g* for 5 min. The cells were transferred to brown tubes and kept in PBS at 4 °C. The intensity of DAF-FM, DCF-DA, and MitoSOX fluorescence was measured by FACSAria III with Diva software (BD Biosciences), and the images were merged using the WinMDI software version 2.8 (Joseph Trotter, http://facs.scripps.edu/software.html).

2.11. Confocal microscopy

RAW264.7 cells were fixed by 3.7% formaldehyde (Sigma-Aldrich) for 5 min and permeabilized with 0.2% Triton X-100 for 5 min. The fixed cells were blocked with 5% FBS (Thermo Scientific) in PBS for 30 min and then incubated with primary antibodies (1:1000, 1 h), targeting p-p65 (Cell Signaling Technology). Next the primary antibody bound-cells were incubated with secondary antibodies (1:1000, 1 h), conjugated with Alexa Fluor 546 (Invitrogen, Carlsbad, CA, USA). Nuclei were stained with Hoechst33258 (5 μM; Sigma-Aldrich) for 10 min. Stained cells were visualized using confocal microscopy (LSM-700, Carl Zeiss Microimaging, Germany) and analyzed by Zen 2009 software.

2.12. In vivo experiments

C57BL/6J mice were obtained from the Orientbio, Korea. TAP2 was reconstituted in PBS at a concentration of 20 pmol/g of animal weight. Eight weeks old mice (group of 6 healthy mice) were treated intraperitoneally with TAP2 for 1 h. The treated mice were then challenged with LPS at a concentration of 5 μg/g of animal weight, for 2 h. Control group (6 mice) received equivalent volume of PBS. The blood plasma samples were collected and analyzed for cytokine secretion. Mouse TNF-α, IL-12p40 and IL-6 were measured using ELISA kits from BioLegend (San Diego, CA). All animal experiments were conducted with approval from the KPC (Gwangju, Gyeonggi-do, Korea) Institutional Animal Care and Use Committee (approval number: P160046).

2.13. Surface plasmon resonance and TLRs-TAPs binding kinetics

SPR experiments were performed using a ProteOn XPR36 instrument (Bio-Rad Laboratories, inc.) with proteOn GLH sensor chip. Phosphate-buffered saline supplemented with 0.05% Tween 20 was used as running buffer and 0.85% phosphoric acid or PBST for regeneration. Human recombinant TLR4/MD2, MD2, TLR2 and TLR1 (R&D systems) were immobilized by amine coupling onto surfaces of a GLH sensor chip as described in protocol. Five different concentrations of TAP2 (0, 1.25, 2.5, 5 and 10 μM) were injected into the chip to check their binding with immobilized proteins. TAP1 was excluded from SPR assay because of its unstable nature (*in silico*), and high concentration requirements for *in vitro* assays and experiments. Running buffer was injected into the empty channel as a reference. The dissociation was monitored for 5 min and the chip was regenerated for the second round. The experiments were performed in duplicates using freshly prepared reagents. ProteOn manager™ software (version 2.0) was used to analyze the data. The binding curves were processed for the start injection alignment and baseline. Reference-subtracted sensorgram was fitted globally to the curves describing a homogeneous 1:1 model. Data from the four protein surfaces were grouped together to fit the kinetic rate constants (k_a and k_d). The equilibrium dissociation constant, kD, was calculated using the equation given below.

$$\mathrm{kD} = k_d / k_a$$

2.14. In silico analysis of the selected TLR4/MD2 modulating peptides

The initial 3D structural models of TAP1, TAP2 and TAP3 oligopeptides were generated through MOE suit and I-TASSER online server [45]. On the basis of the TM score (template-modeling score: an algorithm for the calculation of the similarity of topologies of two protein structures), protein structures showing high similarity and identity to the peptide were selected by I-TASSER for structural alignment and modeling. The 3D structures, showing the same folds and a TM score >0.5 [46], were selected from the top five models of each peptide and were then validated. The overall geometric and stereo-chemical properties of the final 3D-modeled peptides were examined by means of Ramachandran plots generated by MOE (2013.08) and PROCHECK [47]. To assess the binding affinity of the TAPs with the human TLR4/MD2 complex and TLR2, the relevant X-ray crystals, 3FXI and 2Z7X were retrieved from PDB. The LPS, unbound water and PAM3 molecules were removed from the crystal structures and the latter were further inspected for abnormalities using a structural preparation package distributed with MOE. The RsLA, a known TLR4/MD2 antagonist in humans, discussed in our previous study [48], and LPS-TLR4/MD2 were used for comparative interface and binding-energy analysis. Further details about the protein-protein docking and MDS are provided in the supplementary information under heading, supplementary methods.

2.15. Statistical analysis

All the data presented in this work were obtained from at least three independent experiments. The statistical significance was defined by *P* values < 0.05 or <0.01 using the two-tailed paired Student's *t*-test in the SigmaPlot software, version 12.0 (Systat Software Inc., San Jose, CA, USA).

3. Results

3.1. Selection of TLR4/MD2-specific TAPs through Ph.D

To identify TLR4/MD2-specific binding peptides, fUSE55 (for 15-mer TAPs) and pHEN2 (for 12-mer TAPs) Ph.D. libraries were constructed and exposed to a 96-well plate coated with TLR4/MD2. TAP1 (15-mer) was identified in the fUSE55 Ph.D. library after five-round biopanning. TAP2 and TAP3 (12-mers) were identified in the pHEN2 Ph.D. library after five-round biopanning with a hyperphage system. After each round of biopanning, the enrichment level was tested, judging by the titer of the eluted phages (Fig. 1A).

High-throughput screening (HTS) was performed using an enzyme-linked immunosorbent assay (ELISA) to search for independent phage clones that can bind to plate-bound TLR4/MD2 complex; the latter were selected after the fifth round of biopanning. Genomic DNA of the clones showing high binding affinity with TLR4/MD2 were sequenced and aligned through BioEdit [44] to check their identity. Identical sequences were found in different clones and only one sequence was selected from the 15-mer library and two sequences from the 12-mer library. The respective 15-mer and 12-mer TAPs were synthesized by adding front (2 amino acids for 15-mer and 3 amino acids for 12-mer) and rear (3 amino acids for both 15 and 12-mer) residues of the library in order to minimize distortion in the structure (Fig. 1B).

Next, the TLR4 modulating effects of TAPs were evaluated in HEK-Blue™ hTLR4 cells by monitoring the activation of NF-κB and SEAP activity. *Secreted embryonic alkaline phosphatase* (*SEAP*) reporter gene is under the control of the IL-12p40 minimal promoter containing NF-κB- and activator protein 1 (AP-1)-DNA binding sites; IL-12p40 is produced by activation of NF-κB and AP-1 after the stimulation of TLR4. Hence, the activation of TLR4 was measured by means of SEAP activity using different concentrations (10, 50, and 100 μg/ml) of TAPs. The results showed that treatment of cells with only TAPs did not affect SEAP activity, whereas the cells pretreated with TAPs and then stimulated with LPS showed a significant dose-dependent decrease in the LPS-induced SEAP activity (Fig. 1C).

3.2. TAPs negatively regulate LPS-induced TLR4 signaling

After SEAP assay, we next evaluated the TLR4-inhibitory effect of TAPs *in vitro* using mouse macrophages (RAW264.7). TAP1 inhibited inducible nitric oxide synthase (iNOS), IL-6 and NO secretion at 100 μg/ml but could not sustain this effect at lower concentrations. However, TAP2 and TAP3 efficiently retained their TLR4 inhibitory effect at lower concentrations (10–100 ng/ml) (Supplementary Figs. S1A and B). By considering this and evaluating the cell viability (Fig. 2A), further experiments were performed at concentrations of 10–100 μg/ml for TAP1, and 1–100 ng/ml for TAP2 and 3. Further, a dose-dependent effect of TAPs was monitored by evaluating the level of proinflammatory cytokines in 24 h LPS-stimulated RAW264.7 cells. The LPS-induced secretion of IL-6 and NO was significantly suppressed by TAPs in a dose-dependent manner (Fig. 2B and C).

LPS-induced NF-κB activation was also estimated through western blotting in RAW264.7 cells. TAPs inhibited the LPS-induced

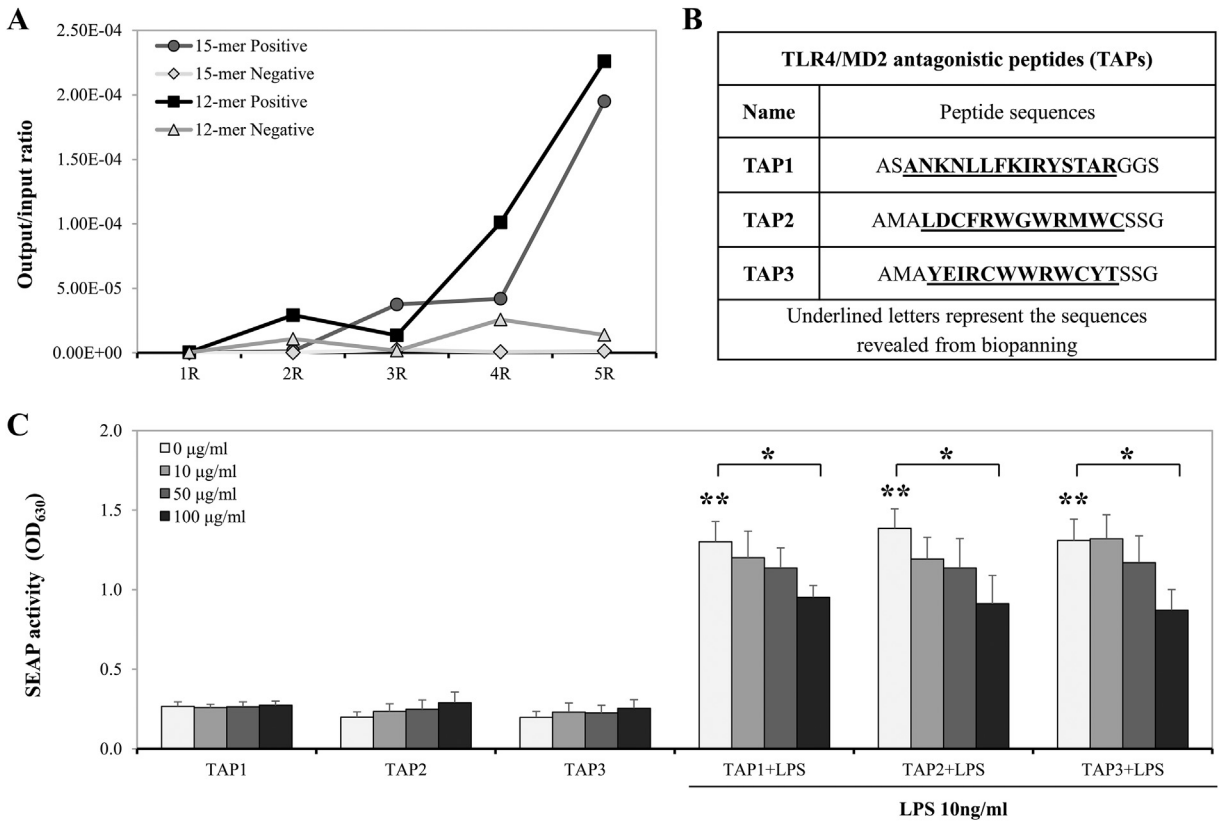

Fig. 1. Screening of the TLR4/MD2-specific small peptides. (**A**) The output/input ratio of biopanning results against the TLR4/MD2 recombinant protein complex from the fUSE55 and pHEN2 phage display libraries. (**B**) The amino acid sequences of the TLR4/MD2-specific binding peptides (TAPs). (**C**) Activation of NF-κB by lipopolysaccharide (LPS) in terms of SEAP activity in HEK-Blue™ hTLR4 cells was measured in response to the LPS-antagonizing peptides (TAPs) at three concentrations: 10, 50, and 100 μg/ml with or without LPS (10 ng/ml). The cells were pretreated with TAPs for 1 h and then treated with LPS (gray bars) or left untreated (white bars) for 24 h. All experiments were independently conducted five times and mean ± SEM of the independent experiments were calculated and used in the two-tailed paired Student's *t*-test (*$P < 0.05$).

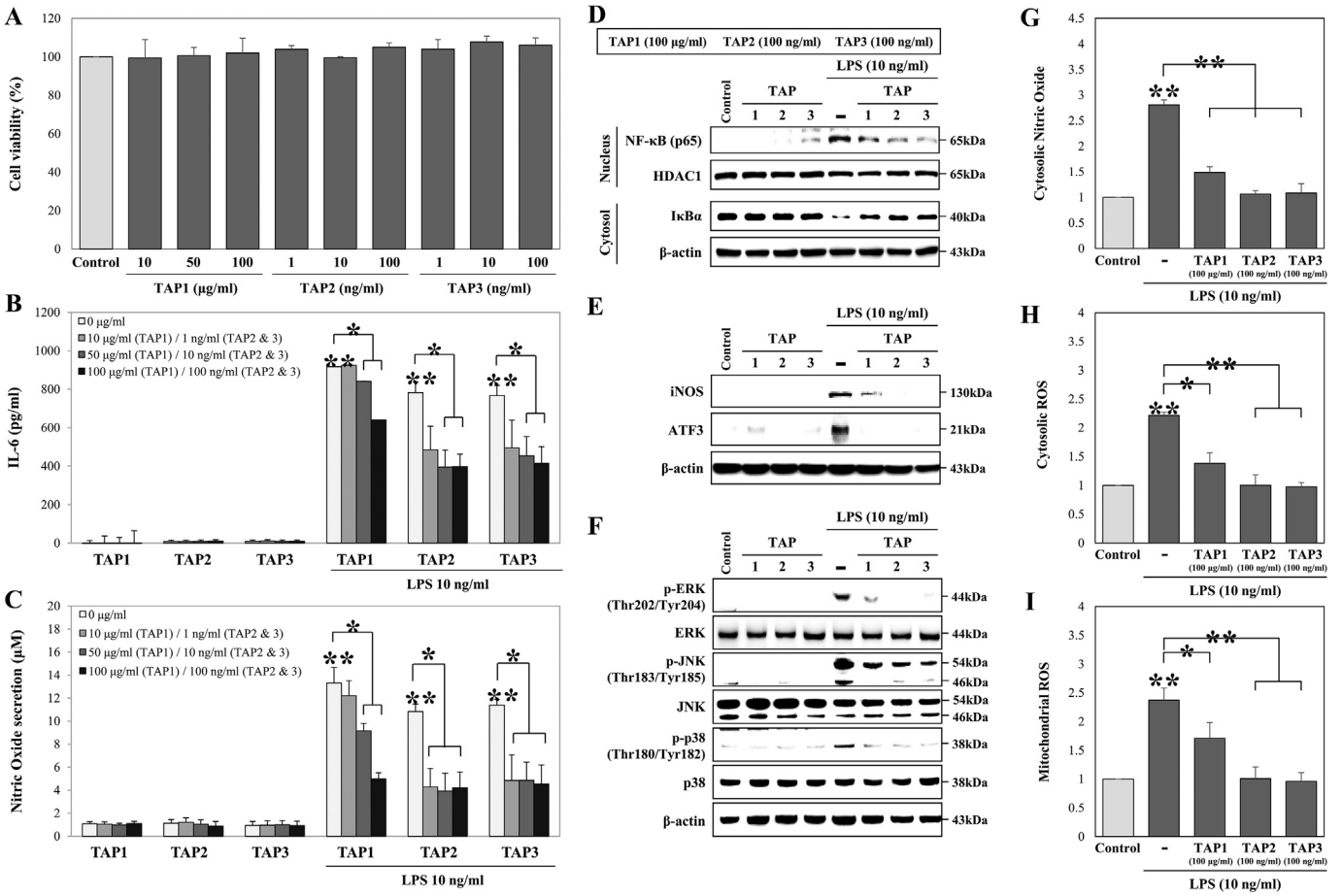

Fig. 2. Suppression of lipopolysaccharide (LPS)-induced proinflammatory response by the TAPs in RAW264.7 cells. (**A**) Cells were treated with various doses of LPS-antagonizing peptides, TAP1 (10, 50, and 100 μg/ml) and TAP2 and 3 (1, 10, and 100 ng/ml) for 24 h. Cell viability were measured by microplate reader using MTT assay. (**B**) Cells were treated with or without various doses of TAPs, TAP1 (10, 50, and 100 μg/ml) and TAP2 and 3 (1, 10, and 100 ng/ml) for 1 h, followed by treatment with LPS (10 ng/ml) for 24 h. The secreted levels of IL-6 (in pg/ml) were measured in the cell culture supernatant by IL-6 ELISA kit. (**C**) The secreted level of NO (in μM) was measured in the cell culture supernatants using the NO detection kit. (**D**) NF-κB activation (NF-κB translocation into the nucleus and degradation of IκBα in the cytosol) was measured by western blotting after cells were incubated with TAP1 (100 μg/ml) TAP2 or TAP3 (100 ng/ml) for 1 h, followed by treatment with LPS (10 ng/ml) for 30 min. (**E**) Expression levels of iNOS and ATF3 were measured by western blot analysis using whole-protein extracts. Cells were incubated with TAP1 (100 μg/ml), TAP2, or TAP3 (100 ng/ml) for 1 h, followed by treatment with LPS (10 ng/ml) for 24 h. (**F**) The activation of MAPKs were measured by western blot analysis after treatment with LPS (10 ng/ml) for 30 min using whole-protein extracts, with inactive MAPKs taken as controls (β-Actin was used as a loading control). (**G**) Cells were incubated with TAP1 (100 μg/ml), TAP2, or TAP3 (100 ng/ml) for 1 h, followed by treatment with LPS (10 ng/ml) for 24 h. The level of NO in the cytosol was measured by fluorescence-activated cell sorting (FACS) with DAF-DA staining. (**H**) Generation of ROS was measured in the cytosol by FACS using DCF-DA staining (**I**) ROS generation in mitochondria was measured by FACS using MitoSOX staining. All experiments were independently conducted three times, and mean ± SEM of the independent experiments were calculated and used in the two-tailed paired Student's *t*-test (*$P < 0.05$).

NF-κB activation and IκBα degradation in RAW264.7 cells in comparison with the cells treated with LPS only (Fig. 2D). Similarly, LPS induced the translocation of NF-κB into the nucleus in comparison with control; this process was inhibited after treatment with TAPs followed by LPS treatment (Supplementary Fig. S2). The western blot results showed that LPS significantly enhanced iNOS expression level, nonetheless, TAPs and LPS co-treated cells showed a decrease in the expression level of iNOS and ATF3; no effect was observed in the cells treated with TAPs only (Fig. 2E; Supplementary Fig. S3). TLRs are known to induce activation of MAPKs: c-Jun N-terminal kinase (JNK), extracellular signal-regulated kinase (ERK), and p38 mitogen-activated protein kinases (p38), which activate the transcription factor AP-1 [2–4]. Furthermore, TLR4 stimulation leads to the induction of activating transcription factor 3 (*ATF3*) and *iNOS* in macrophages [49,50]. Similarly, our results showed that LPS induced the early-phase activation of MAPKs, including phosphorylation of ERK, JNK, and p38 (the formation of p-ERK, p-JNK, and p-p38) in RAW264.7 cells, whereas TAPs inhibited the LPS-induced activation of MAPKs (Fig. 2F; Supplementary Fig. S4). These findings demonstrated that TAPs inhibited the LPS-induced TLR4-mediated activation of NF-κB and MAPK in RAW264.7 cells.

Next, our 4-amino-5-methylamino-2′,7′-difluorofluorescein diacetate (DAF-FM) analyses suggest that TAPs suppress the cytosolic NO generation in the LPS-stimulated RAW264.7 cells (Fig. 2G). Comparatively same results were obtained in the NO secretion assay (Fig. 2C). It has been reported that the LPS-stimulated TLR4 induces ROS generation in cytosol and mitochondria in macrophages and gastric cancer cells [6,51]. For these reasons, the investigation was proceeded to examine the effects of the TAPs on ROS generation. The LPS-induced formation of ROS was examined in the cytosol and mitochondria of RAW264.7 cells treated with TAPs for 24 h, using the 2′,7′-dichlorodihydrofluorescein diacetate (DCF-DA) and MitoSOX staining, which was analyzed by fluorescence-activated cell sorting (FACS). The DCF-DA results suggested that LPS induced generation of ROS in the cytosol, but

this effect was attenuated after co-treatment with TAPs (Fig. 2H). Besides, the MitoSOX staining showed that the LPS-induced generation of ROS in mitochondria decreased after treatment with TAPs (Fig. 2I). Thus, these results showed that TAPs suppressed the LPS-induced generation of oxidative stress markers, such as NO and ROS in macrophages.

3.3. *In silico investigation of TLR4/MD2-modulating TAPs*

The small peptides proposed in this study antagonize the effects of LPS on HEK-BlueTM hTLR4 and RAW264.7 cells. We further investigated the structural features of TAPs, and identified their possible binding mode on TLR4/MD2 complex and proposed their possible LPS antagonizing effect. The modeled structures were simulated in GROMACS and average structures of the TAPs during the last 10 ns were extracted from the MD trajectory after stabilization (Supplementary Fig. S5A). TAP1 has two β-sheets at its N terminus, with a long coil at the C terminus. TAP2 has a helical structure, whereas the average three-dimensional (3D) structure of TAP3 contains two antiparallel β-sheets connected by a loop (Supplementary Fig. S5B). The estimated physiochemical properties of the TAPs, according to the primary protein sequences, are listed in Table S1. The dominant hydrophobic nature of TAP2 and its stable cylindrical structure suggests that it may stably bind to TLR4/MD2 complex, likely to an area that is dominantly occupied by hydrophobic patches. The 3D model of TAP1 suggests that it has a bulky shape with no prominently dominating surface patches and a very unstable structure as compared to TAP2 and TAP3. The docking results (discussed in detail in SI results section) suggest that TAPs preferentially found their way to the MD2 in both TLR4-bound and in unbound form. However, TAP1 seems to exhibit some weak or nonspecific interaction besides interacting with MD2. TAPs-bound TLR4/MD2 complexes were subjected to MDS to investigate their binding stability and structural dynamics (discussed in SI results).

3.4. *Investment of the Phe126 loop in TLR4/MD2-TAPs complexes and interface analysis*

The interfaces of MD2 that are bound to LPS and RsLA were compared with TAPs. The common hydrophobic binding pocket of MD2 for LPS and RsLA showed the binding residues similar to those that bind to TAPs (Fig. 3). To determine the agonist-antagonist switching movement of the Phe126 loop in MD2, the dynamics of MD2-bound TAPs and controls were monitored. As reported previously, the flexible loop containing Phe126 determines the agonistic or antagonistic nature of the ligand that fits into the MD2 pocket (*i.e.*, the solvent-exposed side chain of Phe126 can act as an antagonist and vice versa) [19,52]. To test whether the bound TAPs configurationally direct Phe126 into the solvent, 3D animated videos of the TAP–MD2 complexes were created on the basis of principal component analysis (PCA). Initially, Phe126 interacted with TAP1 or TAP2 and remained on the verge of MD2's pocket but displaced its side chain position by 4.8 Å and 7.6 Å, respectively, into the MD2's pocket when the structure evolved with time (Supplementary Fig. S6; Videos S1 and 2). Besides, the pocket was found to shrink and enclose the bound TAPs inside. In addition to Phe126, Ile124 also showed prominent movements and may be involved in favoring the antagonistic behavior of the bound ligands. Under all the antagonistic scenarios in this study, Ile124 moved toward the MD2-bound TAPs/RsLA, whereas in case of LPS, it moved away from it. We did not observe any prominent movement of Phe126 in TAP3, but Ile124 tended to move toward the bound TAP3 as was observed in TAP1 and TAP2 (Video S3). These findings underscored the importance of the Phe126 loop in TLR4/MD2 modulation and suggested that besides Phe126, Ile124 may play a key role in TLR4 signaling [19,53].

Supplementary video related to this article can be found at http://dx.doi.org/10.1016/j.biomaterials.2017.02.023.

The native function of vital cellular proteins is augmented or abolished by the binding ligands. It has been studied that MD2 is unusually flexible [54] and the clamshell-like motions of its β-cup fold (Videos S1–5), enable it to accommodate the size and shape of the bound ligand into its hydrophobic cavity. These results showed that MD2 utilized this conformational plasticity in a ligand-dependent manner. The peptides in this study are well accommodated in the ligand-binding cavity of the MD2, but its structural dynamics did not show any prominent moment to declare the TLR4-antagonistic nature of these peptides. However, it is easy to understand that the LPS-antagonizing effect of TAPs is likely because they engage the LPS binding to TLR4/MD2 complex.

3.5. *TAP2 specifically binds to TLR4/MD2 as confirmed through biophysical and in vitro assays*

Our initial *in vitro* assays and computational analysis suggested that TAP2 among other TAPs has prominent TLR4-antagonizing effect and could be TLR4-specific as well. To investigate this further, we used surface plasmon resonance (SPR) technique and further *in vitro* assays. SPR can give detailed information on the binding kinetics of a ligand-receptor interaction, without the need for a molecular label, which adds time and extra cost to the assay developed for protein ligand interaction. To investigate the kinetics of the interaction of TAP2 with TLR4/MD2, MD2, TLR2 and TLR1, five different concentrations of TAP2 were passed over immobilized TLRs and MD2 (Fig. 4A and B; Supplementary Figs. S7A and B). TAP2 showed promising results, with a dose dependent increase in its binding to the chip-bound proteins, as indicated in the sensorgram. The calculated k_a and k_d values for TAP2 and TLR4/MD2 binding were, $8.84 \times 10^3\ M^{-1}S^{-1}$ and $5.26 \times 10^{-2}\ S^{-1}$ and their equilibrium dissociation constant (kD) was 5.95 μM. The k_a and k_d values for TAP2 and MD2 interactions were $1.95 \times 10^7\ M^{-1}S^{-1}$ and $1.93 \times 10^2\ S^{-1}$ respectively, and their kD was 9.9 μM. TAP2 did not show any binding with TLR1, however, it binds to TLR2 with three times lower affinity (kD = 17 μM) than it binds to TLR4/MD2 complex.

The TLR4/MD2 specificity of TAP2 was further verified *in vitro*. RAW264.7 cells were treated with TAP2 in combination with various other TLR ligands and the resulting TNF-α level was measured. Interestingly, we found that TAP2 significantly repressed LPS-induced TNF-α in a dose dependent manner, while this suppression was not seen when cells were treated with other TLR ligands, including PAM_3CSK_4 (TLR1/2), FSL-1 (TLR2/6), Poly (I:C) (TLR3), R848 (TLR7/8) and CpG-ODN (TLR9) (Fig. 4C). Additionally, TAP2 significantly decreased expression level of phosphorylated p65 (NF-κB) (indicates NF-κB activation), as suggested by our confocal microscopy results (Fig. 4D). Furthermore, our western blot results also suggested that TAP2 has no effect on the PAM_3CSK_4 (TLR1/2 ligand)-induced NF-κB nuclear translocation and cytosolic degradation of IκBα, as investigated in RAW264.7 cells (Supplementary Fig. S7C). However, this effect was not monitored through western blot technique for other TLR ligands, as was already confirmed in TNF-α assay.

3.6. *TAP2 suppressed NF-κB and MAPKs activation in hPBMC*

As discussed, the selected TAPs were screened through biopanning using recombinant human TLR4/MD2 protein, and further

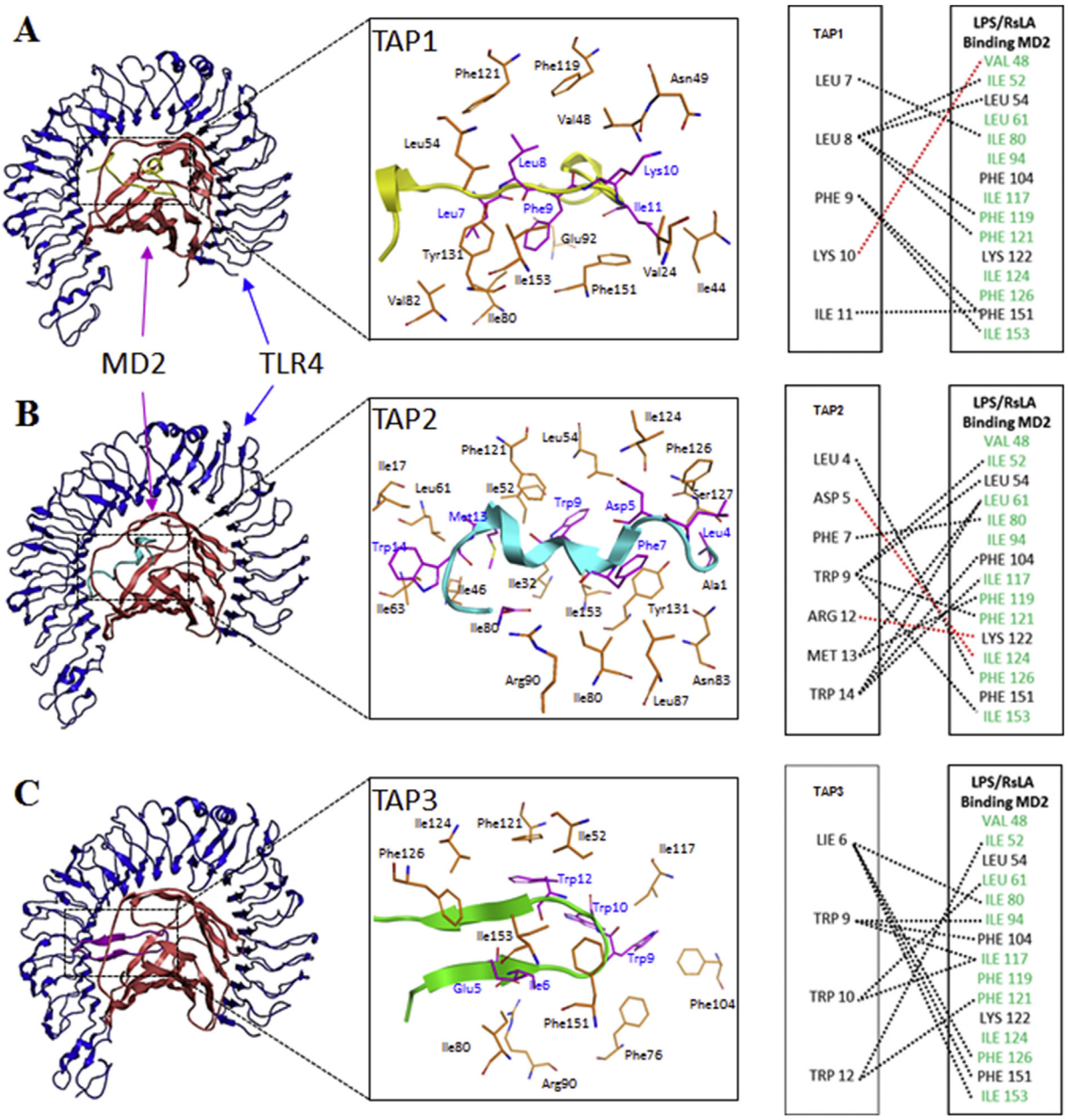

Fig. 3. Comparison of the binding interfaces of MD2-bound TAPs complexes. (**A**) TAP1, (**B**) TAP2, (**C**) TAP3, are bound to the hydrophobic pocket of MD2. The residues in MD2 that bind to LPS and RsLA were studied for comparison with the three peptides (right). Black dotted lines are hydrophobic interactions and red lines are hydrogen bonds. Green residues represent the MD2 residues interacting with both LPS and RsLA, whereas the residues colored in black interact with LPS only. (For interpretation of the references to colour in this figure legend, the reader is referred to the web version of this article.)

confirmed their TLR4-specificity and binding affinity in HEK-Blue hTLR4 cell through SEAP assay. Further experiments were performed in mouse macrophages (RAW264.7). We wished to investigate the TLR4 antagonistic effect of TAP2 in primary human peripheral blood mononuclear cells (hPBMC). As expected, TAP2 had no toxicity and did not affect cells viability at various concentration (Fig. 5A). The expression level of p-p65 was measured through western blotting in TAP2-treated hPBMC. We found that TAP2 substantially repressed the level of LPS-induced p-p65 in cells (Fig. 5B). Furthermore, TAP2 also inhibited the activation level of LPS-induced MAPKs, including ERK, JNK, and p38, as was monitored through western blotting (Fig. 5C).

3.7. TAP2 blocks TLR4 mediated systemic cytokine response in mice

To check the stability and effectiveness of TAP2 *in vivo*, C57BL/6J mice were intraperitoneally (IP) inject with TAP2 and then challenged with LPS at a concentration of 5 μg/g of mouse body weight. Peptide was IP administered at a dose of 20 pmol/g of mouse weight, 1 h before mice were challenged with LPS. TNF-α, IL-12p40 and IL-6 level were measured in blood plasma samples collected immediately before and after LPS stimulation. Predictably, we found that TAP2 pre-treatment significantly decreased the LPS-induced secretion of TNF-α, IL-12p40 and IL-6 in mice models (Fig. 5D). Altogether, these data suggest that TAP2 could be a

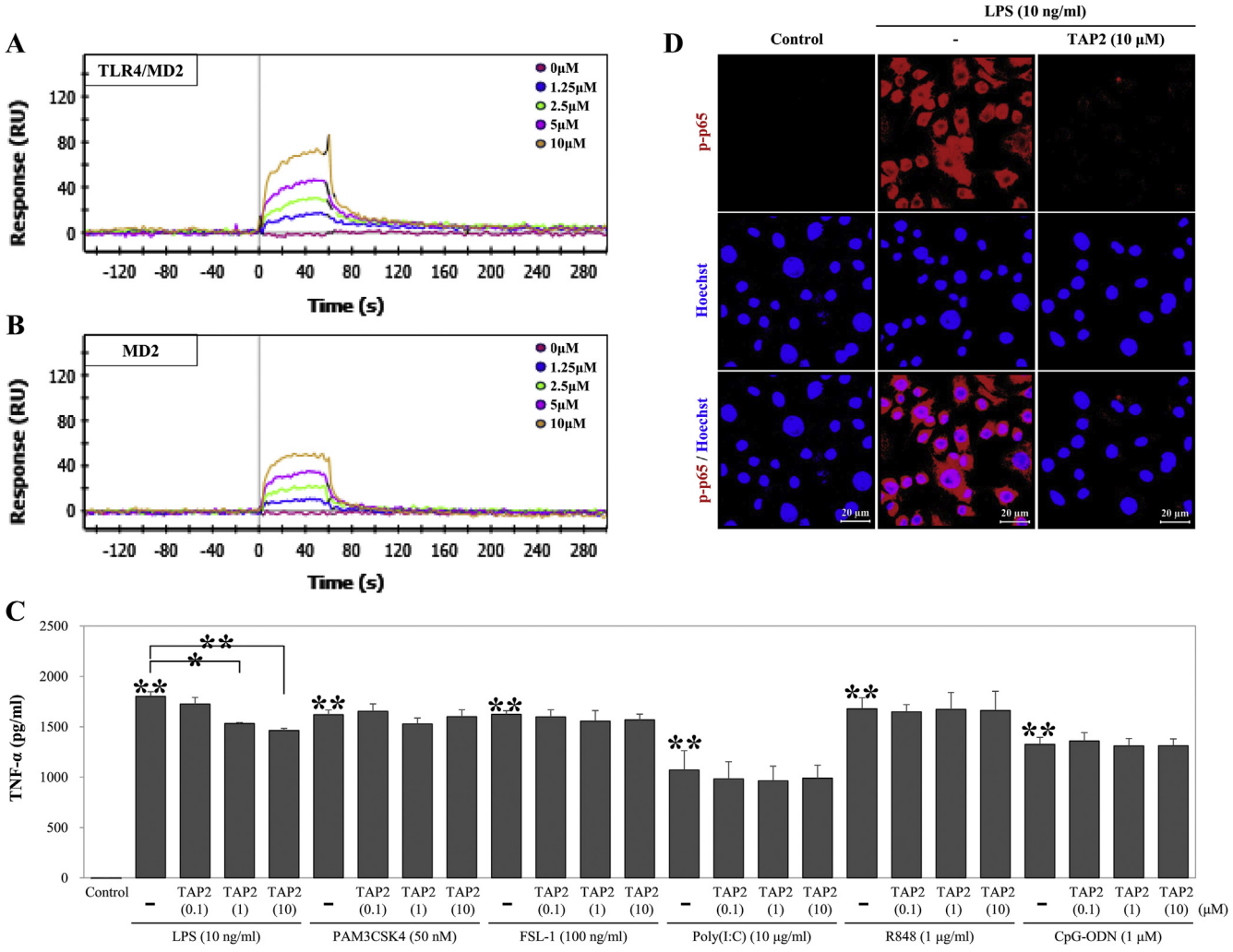

Fig. 4. TAP2-dependent suppression of TNF- α activation in RAW264.7 cells, as induced by multiple TLRs ligands (TLR4/MD2 specificity of TAP2). Immobilization of (**A**) TLR4/MD2 complex and (**B**) MD2, onto a sensor chip and detection of the analyte-bound TAP2 through SPR machine. (**C**) Cells were treated with LPS (10 ng/ml) or PAM_3CSK_4 (50 nM) or FSL-1 (100 ng/ml) or Poly(I:C) (10 μg/ml) or R848 (1 μg/ml) or CpG-ODN (1 μM) for 24 h after TAP2 (0.1, 1, 10 μM) treatment for 1 h. The secreted levels of TNF-α (in pg/ml) were measured in the cell culture supernatant by TNF-α ELISA kit. (**D**) Confocal microscopy showed the phosphorylated NF-κB (p-p65) expression level. The red staining corresponds to phosphorylated NF-κB (p-p65) and blue staining, Hoechst33258, indicates nuclei (the scale bar is 20 μm). All experiments were independently conducted three times and mean ± SEM of the independent experiments were calculated and used in the two-tailed paired Student's *t*-test (*$P < 0.05$). (For interpretation of the references to colour in this figure legend, the reader is referred to the web version of this article.)

promising TLR4/MD2 inhibitor and will help to overcome TLR4-related autoimmune disorders in future.

4. Discussion

Besides providing protection against many microbial and viral infections, TLR4 is known to be involved in the pathogenesis of various neurodegenerative (e.g., Alzheimer's, Parkinson's, and Huntington's diseases) and autoimmune and inflammatory disorders [55–58]. The loss of TLR4 expression and lower ROS production have also been linked to slow the progression of acute lung injury [59]. Similarly, the generation of ROS has been reported to contribute to the pathogenesis of neurodegenerative diseases and cancers [60–62]. Various antagonistic compounds targeting TLRs, in particular TLR4, have been extensively studied to prevent or ameliorate infectious diseases [9].

A small-molecule inhibitor of TLR4, TAK242, which targets the TIR domain of TLR4, has been reported to be responsible for the suppression of the LPS-induced secretion of IL-6 and NO production in RAW264.7 cells [63]. Nevertheless, the use of this inhibitor was stopped in a phase III trial because of safety issues and efficacy concerns (clinical trials identifier: NCT00633477) [9]. A synthetic LPS analogue, eritoran (a TLR4 antagonist) [19], was recently tested in a phase III trial (NCT00334828). Recently, a peptide inhibitor of TLR4 (known as VIPER) was shown to inhibit the LPS-induced IL-6 secretion by targeting adaptor proteins in the TIR domain, for example, MyD88 adapter-like (Mal) and TRAM in RAW264.7 cells [64]. Moreover, in a mouse model of rheumatoid arthritis, heparin nanoparticles (a TLR4-specific inhibitor) suppress the arthritic score, expression of proinflammatory cytokines, the generation of anticollagen antibodies, and NF-κB function [65]. Therefore, the involvement of TLR4 in the onset of many diseases is the reason why TLR4 signaling has been studied so extensively and why the molecules targeting this receptor are being constantly developed; however, clinically effective peptides specifically binding to TLR4 are yet to be identified.

Accordingly, this study was conducted to identify novel TLR4-modulating peptides using the Ph.D. system and investigated

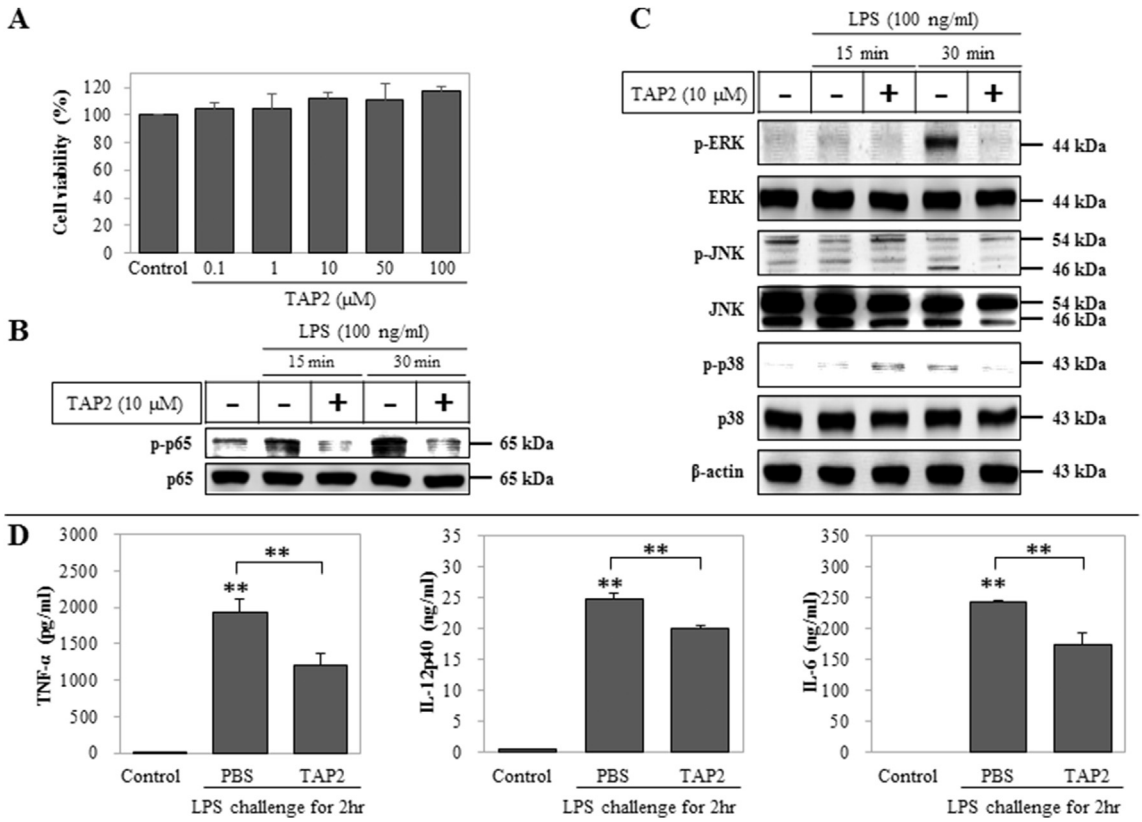

Fig. 5. Inhibitory Effect TAP2 on LPS-induced activation of NF-κB and MAPKs in human peripheral blood mononuclear cells (hPBMCs), and TLR4-dependent cytokines release in mice. (**A**) hPBMCs were treated with TAP2 for 24 h and the cell viability was measured using MTT assay. (**B**) The expression level of phosphorylated p65 (p-p65) was measured by western blotting after hPBMCs were incubated with TAP2 for 1 h, followed by treatment with LPS (100 ng/ml) for 15 and 30 min. (**C**) The activation of MAPKs were measured by western blot analyses using whole-protein extracts. Inactive MAPKs were taken as controls (β-Actin was used as a loading control). (**D**) Inhibitory effect of TAP2 on LPS-induced TLR4-dependent cytokine secretion in Mice. Mice were intraperitoneally (IP) treated with PBS (control) or with 20 pmol/g of TAP2 1 h before IP administration of LPS (5 μg/g). Plasma samples were obtained from six mice in each group (control and TAP2-treated). Numerical data are presented as means ± SEM (*P < 0.05, **P < 0.01 compared to the control or PBS).

their effect on the downstream signaling mechanism of TLR4. Since its inception, the Ph.D. method has been a promising approach for rapid screening of large numbers of peptides. Using this method, millions of small peptides were screened from two libraries and three TLR4/MD2-specific candidate peptides were identified, which were further validated in empirical experiments. As a preliminary test, HEK-Blue™ hTLR4 cells were used to monitor the TLR4 (in) activation via SEAP; these experiments indicate that these peptides block TLR4 activation (Fig. 1C). Treatment of RAW264.7 cells with these peptides inhibited the TLR4-induced secretion of IL-6 and NO in a dose-dependent manner (Fig. 2B and C). TAPs reduced the IκB degradation, eventually delayed the NF-κB nuclear translocation and prevented the activation of MAPKs (Fig. 2D, F). iNOS, NO and ROS, correlated with oxidative stress, are induced after TLR4 activation [50], but a significant decrease in the levels of these substances was observed after TAPs treatment (Fig. 2E,G–I).

Most but not all of the extracellular ligands of TLR4 have been shown to bind to MD2's pocket that either activate or inhibit the downstream signaling [18,19]. To investigate the structural features, stability and possible binding position on TLRs and MD2, TAPs were modeled and docked, using different servers and software packages. The most plausible binding conformations were subjected to further analysis. Molecular dynamics simulations were performed on different complexes and final average snapshots were analyzed in detail to identify the key amino acid residues (Fig. 3A–C). The important interacting residues were found largely in line with various mutational studies [18,19,53]. Another research group reported the identification of a peptide that specifically binds to the MD2-binding region of TLR4. This binding was deciphered via a computational approach and *in vitro* techniques, and the results suggested that this peptide competitively hinders the binding of MD2 to TLR4 [26]. This is likely because the peptide was derived from the TLR4-interacting part of MD2. Nevertheless, this peptide has not been tested *in vivo*. In contrast, Toshchakov's group is actively involved in the development of TLR-inhibiting small peptides derived from the TIR domain of TLR2 and the adapter molecules TIRAP and TRAM. These peptides target the TIR domains of TLR or engage the adapter molecules [36,66,67]. Our results suggest that TAPs most likely bind to the LPS-binding pocket of MD2. In addition, the MAL- and TIR-derived peptides inhibit the signaling of multiple TLRs, whereas TAPs specifically inhibit TLR4 signaling.

SPR technology is extensively utilized to achieve a quantitative ranking of the interaction affinities and the active concentration of protein-interacting ligands and peptides, which can be valuable in drug discovery [68]. The same technique was used to investigate the TLR-binding specificity of TAP2 and its binding kinetics as well. TAP2 was passed over TLR4/MD2, MD2, TLR2 and TLR1 (having different pI values) proteins bound to GLH sensor chip. The binding kinetics of TAP2 showed high binding affinity with MD2 and TLR4/MD2 complex (Fig. 4A and B). The difference in kD values indicate that the binding affinity of TAP2 is higher with TLR4/MD2 than MD2 alone. This phenomenon can be explained by the fact that expression and purification methods of protein play a major role in their structural integrity and ligand binding ability [69]. Since TLR4

does not express on the cell surface alone and needs LPS-induced MD2-mediated hetrodimerization [70,71]; we suggest that TAP2 antagonizes LPS by binding to TLR4/MD2 complex, likely into the MD2 pocket. To confirm the exact binding pattern of TAP2 with TLR4/MD2, further detail structural studies such as NMR or X-ray diffraction would be obliging. Moreover, confocal microscopy analysis strongly suggest that the activation and nuclear translocation of NF-κB inversely correlates with the TAP2 treatment (Supplementary Fig. S2). TAP2 identified in this study is likely specific to TLR4, because no off-target effects of TAP2 were observed when tested for the modulation of TLR1/2, 2/6, 3, 7/8 and 9 signaling (Fig. 4C; Supplementary Fig. S7C). TAP2 was also able to block the activation of NF-κB and MAPKs in hPBMC, and potently suppressed the activation of systemic cytokines in mice, challenged with LPS (Fig. 5D).

5. Conclusion

We believe that TAPs can block both, MyD88- and TRIF-dependent pathways of TLR4 by antagonizing the effect of LPS. LPS can induce the production of iNOS through both, MyD88-dependent and independent pathway; however, TAPs can block the production of iNOS and ultimately the generation of NO. These peptides were tested *in vitro*, *in silico*, and *in vivo* and were found to actively block the LPS-induced TLR4-mediated proinflammatory cytokines and reactive oxygen species. Further, we found that these peptides do not affect other TLRs' pathways, but TLR4. Taken together, our findings suggest that these small peptides are promising candidates for the development of TLR4-specific therapeutics to treat various neurodegenerative and autoimmune diseases.

Competing financial interests

The authors declare that there are no conflicts of interest.

Acknowledgments

This work was supported by the Mid-Career Researcher Program through the National Research Foundation of Korea (NRF-2015R1A2A2A09001059) and the Korea Health Technology R&D Project through the Korea Health Industry Development Institute (HI14C1992). This work was also partially supported by a grant from the Priority Research Centers Program (NRF 2012-0006687).

Appendix A. Supplementary data

Supplementary data related to this article can be found at http://dx.doi.org/10.1016/j.biomaterials.2017.02.023.

References

[1] C.C. Lee, A.M. Avalos, H.L. Ploegh, Accessory molecules for Toll-like receptors and their function, Nat. Rev. Immunol. 12 (2012) 168–179.
[2] K. Takeda, T. Kaisho, S. Akira, Toll-like receptors, Annu. Rev. Immunol. 21 (2003) 335–376.
[3] L.A. O'Neill, D. Golenbock, A.G. Bowie, The history of Toll-like receptors - redefining innate immunity, Nat. Rev. Immunol. 13 (2013) 453–460.
[4] S. Akira, K. Takeda, Toll-like receptor signalling, Nat. Rev. Immunol. 4 (2004) 499–511.
[5] K. Takeda, S. Akira, Toll-like receptors in innate immunity, Int. Immunol. 17 (2005) 1–14.
[6] A.P. West, I.E. Brodsky, C. Rahner, D.K. Woo, H. Erdjument-Bromage, P. Tempst, et al., TLR signalling augments macrophage bactericidal activity through mitochondrial ROS, Nature 472 (2011) 476–480.
[7] C. Cole, S. Thomas, H. Filak, P.M. Henson, L.L. Lenz, Nitric oxide increases susceptibility of Toll-like receptor-activated macrophages to spreading Listeria monocytogenes, Immunity 36 (2012) 807–820.
[8] M.J. Jimenez-Dalmaroni, M.E. Gerswhin, I.E. Adamopoulos, The critical role of toll-like receptors–From microbial recognition to autoimmunity: a comprehensive review, Autoimmun. Rev. 15 (2016) 1–8.
[9] E.J. Hennessy, A.E. Parker, L.A. O'Neill, Targeting Toll-like receptors: emerging therapeutics? Nat. Rev. Drug Discov. 9 (2010) 293–307.
[10] L.A. O'Neill, C.E. Bryant, S.L. Doyle, Therapeutic targeting of Toll-like receptors for infectious and inflammatory diseases and cancer, Pharmacol. Rev. 61 (2009) 177–197.
[11] A. Marshak-Rothstein, Toll-like receptors in systemic autoimmune disease, Nat. Rev. Immunol. 6 (2006) 823–835.
[12] D.N. Cook, D.S. Pisetsky, D.A. Schwartz, Toll-like receptors in the pathogenesis of human disease, Nat. Immunol. 5 (2004) 975–979.
[13] S. Rakoff-Nahoum, R. Medzhitov, Toll-like receptors and cancer, Nat. Rev. Cancer 9 (2009) 57–63.
[14] M. Shah, M.A. Anwar, J.H. Kim, S. Choi, Advances in antiviral therapies targeting toll-like receptors, Expert Opin. Investig. Drugs 25 (2016) 437–453.
[15] M.C. Patra, S. Choi, Recent progress in the development of Toll-like receptor (TLR) antagonists, Expert Opin. Ther. Pat. 26 (2016) 719–730.
[16] F. Peri, M. Piazza, Therapeutic targeting of innate immunity with Toll-like receptor 4 (TLR4) antagonists, Biotechnol. Adv. 30 (2012) 251–260.
[17] X. Wang, C. Smith, H. Yin, Targeting Toll-like receptors with small molecule agents, Chem. Soc. Rev. 42 (2013) 4859–4866.
[18] B.S. Park, D.H. Song, H.M. Kim, B.S. Choi, H. Lee, J.O. Lee, The structural basis of lipopolysaccharide recognition by the TLR4-MD-2 complex, Nature 458 (2009) 1191–1195.
[19] H.M. Kim, B.S. Park, J.I. Kim, S.E. Kim, J. Lee, S.C. Oh, et al., Crystal structure of the TLR4-MD-2 complex with bound endotoxin antagonist Eritoran, Cell 130 (2007) 906–917.
[20] B.W. Jarvis, H. Lichenstein, N. Qureshi, Diphosphoryl lipid A from Rhodobacter sphaeroides inhibits complexes that form in vitro between lipopolysaccharide (LPS)-binding protein, soluble CD14, and spectrally pure LPS, Infect. Immun. 65 (1997) 3011–3016.
[21] F. Peri, V. Calabrese, Toll-like receptor 4 (TLR4) modulation by synthetic and natural compounds: an update, J. Med. Chem. 57 (2014) 3612–3622.
[22] Y. Wang, L. Su, M.D. Morin, B.T. Jones, L.R. Whitby, M.M. Surakattula, et al., TLR4/MD-2 activation by a synthetic agonist with no similarity to LPS, Proc. Natl. Acad. Sci. U. S. A. 113 (2016) E884–E893.
[23] S.E. Hussey, H. Liang, S.R. Costford, A. Klip, R.A. DeFronzo, A. Sanchez-Avila, et al., TAK-242, a small-molecule inhibitor of Toll-like receptor 4 signalling, unveils similarities and differences in lipopolysaccharide- and lipid-induced inflammation and insulin resistance in muscle cells, Biosci. Rep. 33 (2012) 37–47.
[24] N. Matsunaga, N. Tsuchimori, T. Matsumoto, M. Ii, TAK-242 (resatorvid), a small-molecule inhibitor of Toll-like receptor (TLR) 4 signaling, binds selectively to TLR4 and interferes with interactions between TLR4 and its adaptor molecules, Mol. Pharmacol. 79 (2011) 34–41.
[25] A. Shanmugam, S. Rajoria, A.L. George, A. Mittelman, R. Suriano, R.K. Tiwari, Synthetic Toll like receptor-4 (TLR-4) agonist peptides as a novel class of adjuvants, PLoS One 7 (2012) e30839.
[26] P.F. Slivka, M. Shridhar, G.I. Lee, D.W. Sammond, M.R. Hutchinson, A.J. Martinko, et al., A peptide antagonist of the TLR4-MD2 interaction, Chembiochem 10 (2009) 645–649.
[27] Q.W. Yang, L. Mou, F.L. Lv, P.F. Zhu, Z.G. Wang, J.X. Jiang, et al., Novel TLR4-antagonizing peptides inhibit LPS-induced release of inflammatory mediators by monocytes, Biochem. Biophys. Res. Commun. 329 (2005) 846–854.
[28] S.S. Sidhu, H.B. Lowman, B.C. Cunningham, J.A. Wells, Phage display for selection of novel binding peptides, Methods Enzymol. 328 (2000) 333–363.
[29] L. Rahbarnia, S. Farajnia, H. Babaei, J. Majidi, K. Veisi, V. Ahmadzadeh, et al., Evolution of phage display technology: from discovery to application, J. Drug Target (2016) 1–9.
[30] K. Omidfar, M. Daneshpour, Advances in phage display technology for drug discovery, Expert Opin. Drug Discov. 10 (2015) 651–669.
[31] G.P. Smith, Filamentous fusion phage: novel expression vectors that display cloned antigens on the virion surface, Science 228 (1985) 1315–1317.
[32] A.A. Alizadeh, M. Hamzeh-Mivehroud, M. Farajzadeh, S. Dastmalchi, Identification of novel peptides against TNF-alpha using phage display technique and in silico modeling of their modes of binding, Eur. J. Pharm. Sci. 96 (2016) 490–498.
[33] Z. Yan, Y. Wu, J. Du, G. Li, S. Wang, W. Cao, et al., A novel peptide targeting Clec9a on dendritic cell for cancer immunotherapy, Oncotarget 7 (2016) 40437–40450.
[34] G. Kubas, W. Rees, J. Caguiat, D. Asch, D. Fagan, P. Cortes, Identification of peptide sequences that selectively bind to pentaerythritol trinitrate hemisuccinate -a surrogate of PETN, via phage display technology, Biopolymers (2016), http://dx.doi.org/10.1002/bip.22997.
[35] Y. Hou, X.X. Gu, Development of peptide mimotopes of lipooligosaccharide from nontypeable Haemophilus influenzae as vaccine candidates, J. Immunol. 170 (2003) 4373–4379.
[36] W. Piao, S.N. Vogel, V.Y. Toshchakov, Inhibition of TLR4 signaling by TRAM-derived decoy peptides in vitro and in vivo, J. Immunol. 190 (2013) 2263–2272.
[37] L. Otvos Jr., J.D. Wade, Current challenges in peptide-based drug discovery, Front. Chem. 2 (2014) 62.
[38] L. Gentilucci, R. De Marco, L. Cerisoli, Chemical modifications designed to improve peptide stability: incorporation of non-natural amino acids, pseudo-peptide bonds, and cyclization, Curr. Pharm. Des. 16 (2010) 3185–3203.

[39] G. Bhardwaj, V.K. Mulligan, C.D. Bahl, J.M. Gilmore, P.J. Harvey, O. Cheneval, et al., Accurate de novo design of hyperstable constrained peptides, Nature 538 (2016) 329–335.
[40] S. Patil, I. Vhora, J. Amrutiya, R. Lalani, A. Misra, Role of nanotechnology in delivery of protein and peptide drugs, Curr. Pharm. Des. 21 (2015) 4155–4173.
[41] B. Zuo, J. Yang, F. Wang, L. Wang, Y. Yin, J. Dan, et al., Influences of lamin A levels on induction of pluripotent stem cells, Biol. Open 1 (2012) 1118–1127.
[42] R. Tonikian, Y. Zhang, C. Boone, S.S. Sidhu, Identifying specificity profiles for peptide recognition modules from phage-displayed peptide libraries, Nat. Protoc. 2 (2007) 1368–1386.
[43] G. Winter, A.D. Griffiths, R.E. Hawkins, H.R. Hoogenboom, Making antibodies by phage display technology, Annu. Rev. Immunol. 12 (1994) 433–455.
[44] H. TA, BioEdit: a user-friendly biological sequence alignment editor and analysis program for Windows 95/98/NT, in: Nucleic Acids Symposium Series, 1999, pp. 95–98.
[45] Y. Zhang, I-TASSER server for protein 3D structure prediction, BMC Bioinforma. 9 (2008) 40.
[46] J.U. Bowie, R. Luthy, D. Eisenberg, A method to identify protein sequences that fold into a known three-dimensional structure, Science 253 (1991) 164–170.
[47] R.A. Laskowski, J.A. Rullmannn, M.W. MacArthur, R. Kaptein, J.M. Thornton, AQUA and PROCHECK-NMR: programs for checking the quality of protein structures solved by NMR, J. Biomol. NMR 8 (1996) 477–486.
[48] M.A. Anwar, S. Panneerselvam, M. Shah, S. Choi, Insights into the species-specific TLR4 signaling mechanism in response to Rhodobacter sphaeroides lipid A detection, Sci. Rep. 5 (2015) 7657.
[49] M. Gilchrist, V. Thorsson, B. Li, A.G. Rust, M. Korb, J.C. Roach, et al., Systems biology approaches identify ATF3 as a negative regulator of Toll-like receptor 4, Nature 441 (2006) 173–178.
[50] E.Y. Kim, H.Y. Shin, J.Y. Kim, D.G. Kim, Y.M. Choi, H.K. Kwon, et al., ATF3 plays a key role in Kdo2-lipid A-induced TLR4-dependent gene expression via NF-kappaB activation, PLoS One 5 (2010) e14181.
[51] X. Yuan, Y. Zhou, W. Wang, J. Li, G. Xie, Y. Zhao, et al., Activation of TLR4 signaling promotes gastric cancer progression by inducing mitochondrial ROS production, Cell Death Dis. 4 (2013) e794.
[52] U. Ohto, K. Fukase, K. Miyake, Y. Satow, Crystal structures of human MD-2 and its complex with antiendotoxic lipid IVa, Science 316 (2007) 1632–1634.
[53] M. Muroi, K. Tanamoto, Structural regions of MD-2 that determine the agonist-antagonist activity of lipid IVa, J. Biol. Chem. 281 (2006) 5484–5491.
[54] T. Paramo, T.J. Piggot, C.E. Bryant, P.J. Bond, The structural basis for endotoxin-induced allosteric regulation of the Toll-like receptor 4 (TLR4) innate immune receptor, J. Biol. Chem. 288 (2013) 36215–36225.
[55] E. Cario, Toll-like receptors in inflammatory bowel diseases: a decade later, Inflamm. Bowel Dis. 16 (2010) 1583–1597.
[56] M.T. Heneka, M.P. Kummer, E. Latz, Innate immune activation in neurodegenerative disease, Nat. Rev. Immunol. 14 (2014) 463–477.
[57] M.H. Wenink, K.C. Santegoets, M.F. Roelofs, R. Huijbens, H.J. Koenen, R. van Beek, et al., The inhibitory Fc gamma IIb receptor dampens TLR4-mediated immune responses and is selectively up-regulated on dendritic cells from rheumatoid arthritis patients with quiescent disease, J. Immunol. 183 (2009) 4509–4520.
[58] E. Okun, K.J. Griffioen, J.D. Lathia, S.C. Tang, M.P. Mattson, T.V. Arumugam, Toll-like receptors in neurodegeneration, Brain Res. Rev. 59 (2009) 278–292.
[59] Y. Imai, K. Kuba, G.G. Neely, R. Yaghubian-Malhami, T. Perkmann, G. van Loo, et al., Identification of oxidative stress and Toll-like receptor 4 signaling as a key pathway of acute lung injury, Cell 133 (2008) 235–249.
[60] J. Lotharius, P. Brundin, Pathogenesis of Parkinson's disease: dopamine, vesicles and alpha-synuclein, Nat. Rev. Neurosci. 3 (2002) 932–942.
[61] B. Uttara, A.V. Singh, P. Zamboni, R.T. Mahajan, Oxidative stress and neurodegenerative diseases: a review of upstream and downstream antioxidant therapeutic options, Curr. Neuropharmacol. 7 (2009) 65–74.
[62] C.A. Ross, E.H. Aylward, E.J. Wild, D.R. Langbehn, J.D. Long, J.H. Warner, et al., Huntington disease: natural history, biomarkers and prospects for therapeutics, Nat. Rev. Neurol. 10 (2014) 204–216.
[63] M. Ii, N. Matsunaga, K. Hazeki, K. Nakamura, K. Takashima, T. Seya, et al., A novel cyclohexene derivative, ethyl (6R)-6-[N-(2-Chloro-4-fluorophenyl) sulfamoyl]cyclohex-1-ene-1-carboxylate (TAK-242), selectively inhibits toll-like receptor 4-mediated cytokine production through suppression of intracellular signaling, Mol. Pharmacol. 69 (2006) 1288–1295.
[64] T. Lysakova-Devine, B. Keogh, B. Harrington, K. Nagpal, A. Halle, D.T. Golenbock, et al., Viral inhibitory peptide of TLR4, a peptide derived from vaccinia protein A46, specifically inhibits TLR4 by directly targeting MyD88 adaptor-like and TRIF-related adaptor molecule, J. Immunol. 185 (2010) 4261–4271.
[65] H. Babazada, F. Yamashita, M. Hashida, Suppression of experimental arthritis with self-assembling glycol-split heparin nanoparticles via inhibition of TLR4-NF-kappaB signaling, J. Control Release 194 (2014) 295–300.
[66] L.A. Couture, W. Piao, L.W. Ru, S.N. Vogel, V.Y. Toshchakov, Targeting Toll-like receptor (TLR) signaling by Toll/interleukin-1 receptor (TIR) domain-containing adapter protein/MyD88 adapter-like (TIRAP/Mal)-derived decoy peptides, J. Biol. Chem. 287 (2012) 24641–24648.
[67] W. Piao, K.A. Shirey, L.W. Ru, W. Lai, H. Szmacinski, G.A. Snyder, et al., A decoy peptide that disrupts TIRAP recruitment to TLRs is protective in a Murine model of Influenza, Cell Rep. 11 (2015) 1941–1952.
[68] W. Huber, F. Mueller, Biomolecular interaction analysis in drug discovery using surface plasmon resonance technology, Curr. Pharm. Des. 12 (2006) 3999–4021.
[69] X. Wang, L.C. Loram, K. Ramos, A.J. de Jesus, J. Thomas, K. Cheng, et al., Morphine activates neuroinflammation in a manner parallel to endotoxin, Proc. Natl. Acad. Sci. U. S. A. 109 (2012) 6325–6330.
[70] Y. Nagai, S. Akashi, M. Nagafuku, M. Ogata, Y. Iwakura, S. Akira, et al., Essential role of MD-2 in LPS responsiveness and TLR4 distribution, Nat. Immunol. 3 (2002) 667–672.
[71] R. Shimazu, S. Akashi, H. Ogata, Y. Nagai, K. Fukudome, K. Miyake, et al., MD-2, a molecule that confers lipopolysaccharide responsiveness on Toll-like receptor 4, J. Exp. Med. 189 (1999) 1777–1782.